International Journal of Microwave and Wireless Technologies, 2017, 9(4), 729–739.
doi:10.1017/S1759078716000933

RESEARCH PAPER

Interference cancellation for higher harmonics of supply-modulated efficient RF power amplifier systems

MOHAMMAD OMER[1] AND FARASAT MUNIR[2]

In building highly efficient transmitters of today, one is forced to sacrifice linearity for efficiency. Some of the highest power amplifier efficiency figures are reported by envelope tracking (ET) amplifiers. These amplifiers can generate strong higher-order harmonics, which can lead to interference with receivers operating at the harmonic frequencies. Using non-linear interference cancellation, we can help to remove the interference being caused in those receivers. This paper looks at the problem of modeling the third and second-order harmonic emission from an ET amplifier. It derives the non-linear kernel for estimating such interference. This kernel has been rigorously expanded to show its correlation with the various harmonics and its effectiveness in predicting the harmonic content. We then set up an envelope amplifier test-bench to capture harmonic signal content and cancel it using the derived kernel model. The experiment yields excellent agreement with theory and provides a validation of the system and concept.

Keywords: Power amplifiers, Digital pre-distortion, Interference cancellation, Modeling, Nonlinear kernels, Adaptive filters, Least squares estimation, Recursive least squares, Surface acoustic wave filters

Received 24 November 2015; Revised 19 July 2016; Accepted 20 July 2016; first published online 18 August 2016

I. INTRODUCTION AND SYSTEM CONCEPT

The transceivers of today are populated with different types of radios and the efficiency of transmitter (*Tx*) is becoming increasingly important to conserve battery life. The highest efficiency demands highly non-linear power amplifier (PA) architectures of which envelope tracking (ET) amplifiers have yielded good results [1]. An ET amplifier uses the information in the envelope to modulate the power supply voltage of the PA and hence force the PA into its most efficient operating point. This modulation of the power supply can yield significant higher-order harmonics. The situation is shown in Fig. 1. We see that the ET system produces an output signal centered at the transmit frequency f_{Tx}. The signal is suffering from spectral expansion due to non-linearities, which produce close-in spectral regrowth as demonstrated by adjacent channel shoulders. However, the non-linearities also produce harmonic distortion at far-off frequencies like $3f_{Tx}$. With many radios operating in parallel on the same platform, a receiver (*Rx*) within the same system may be operating at this far-off frequency. Figure 1 shows a receiver operating close to that frequency. For a receiver tuned close to the frequency of the third harmonic, as long as the operating frequency of the receiver is within three times the bandwidth of the original base-band signal, the receiver can possibly be impacted by the spectral emission at harmonics of f_{Tx}. The close-in spectral regrowth has been extensively studied in the literature [2–4] and non-linear models for it have been developed. Interference cancellation techniques have also been proposed for this kind of spurious emission [5–7]. The emission at harmonic frequencies has however not received attention.

A surface acoustic wave (SAW) filter can provide heavy attenuation at harmonic frequencies to reduce the interference content. This would be a brute force approach to making such systems work. A more analytical approach is to study this harmonic emission, and come up with models to generate this content.

SAW filters in different forms (either as *Tx*/*Rx* duplexers or *Rx* only filters) lead to several major trade-offs in transceiver architectures [8–9]. They impose size, area, power consumption constraint on the transceiver, which hampers both the flexibility of radio front-end, as well as key power performance metrics. Different SAW-duplexers/filters have to be designed to cover different bands, which lead to bill of materials and area costs on the transceiver. A simple calculation can reveal the trade-offs involved. Suppose the transmitter is required to output a power at the antenna of 23 dBm. A duplexer-SAW device (plus extra SAW filtering) may be required to provide enough attenuation to the transmitted spectrum to have acceptable noise/distortion levels at the receiver. If we assume that the duplexer-SAW device is providing the entire attenuation required at the receiver, we can account for the insertion loss (IL) caused by such a setup. A SAW

[1]Cognitive Systems Corp, Canada
[2]Department of Electrical Engineering, LUMS SBA School of Science and Engineering, DHA, Lahore
Corresponding author:
F. Munir
Email: farasat.munir@lums.edu.pk

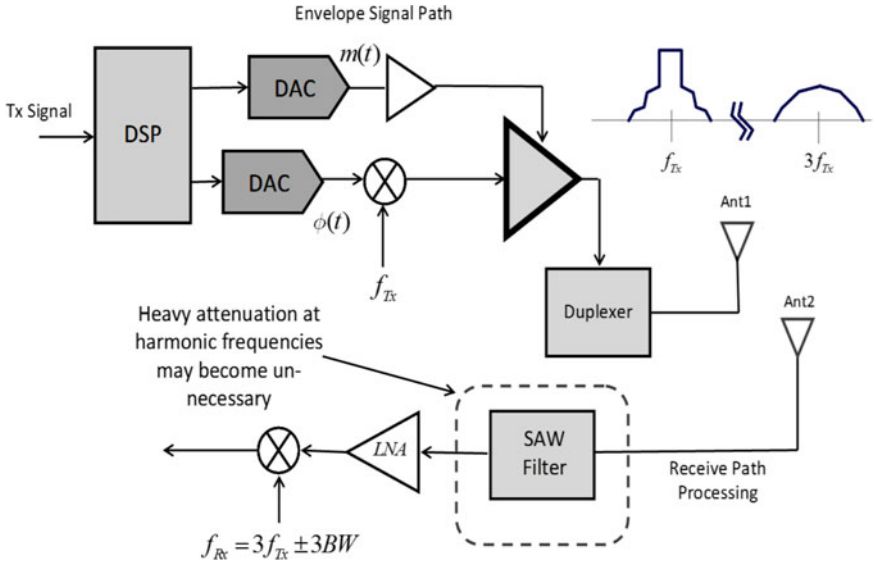

Fig. 1. Impact of Envelope Tracking Amplifier on collocated receiver.

duplexer has an IL typically ranging from 2 to 3 dB. Assuming an IL of 2.7 dB, the PA would have to be driven at a higher output power of 25.7 dBm to deliver the desired output power. The difference in power translates to an extra 172 mW power drawn from the supply rails to deliver the extra radio frequency (RF) power only. For this calculation, we neglect the effect of PA efficiency, which can lead to an extra factor of 1.4–1.6 times on the drawn power. Now we could employ a SAW-duplexer offering lesser isolation, and correspondingly lesser IL. If a compromise on isolation of 10–15 dB is made, the IL of a duplexer can be reduced by 0.5–1 dB [10]. A 0.7 dB improvement in IL will correspond to a power hit of only 117 mW. That means an additional 55 mW of power can be saved just at the transmitter by compromising on the isolation provided by SAW device. The power saving, however, will come at a price. The reduction in isolation will lead to spurious harmonic emissions at the receiver, of up to 15 dB, which would need to be cancelled. We propose and show in this paper that the digital logic comprising of adaptive cancellation algorithms can remove this spurious emission and offer the cancellation of up to 15 dB of *Tx* harmonic emission at the receiver. Also the cancellation circuits can operate at a very low-power consumption totaling up to 2 mW, which is just 3.6% of the power budget required in the case of a more lossy/heavier attenuation duplexer. The digital circuit also achieves a potential size reduction as opposed to a lossier, bulkier duplexer. We provide details on the implementation, tuning, and synthesized power consumption of our adaptive digital cancellation circuits.

Physically it is helpful to think of the amplifier operation as consisting of a cascade of non-linearities as shown in Fig. 2. The switching non-linearity being applied to the (predominantly) phase representation of the signal will create harmonics separated by integer multiples of f_{Tx}. The non-linear harmonics in frequency domain are therefore shown separated by large offsets from each other in Fig. 2. The second non-linear interaction is owing to the compressive characteristics imposed by the supply modulation. These include non-linear interactions that are lower-order polynomials leading to the close-in spectral expansion. Although it is helpful to think of the amplifier operation in this fashion, the actual physical interactions in the supply modulated amplifiers are much more complex [11–13], and have been under continuous investigations in recent years. Our focus in this work is to model these interactions at the mathematical level, and provide analytical description of harmonics at integer multiples of f_{Tx}.

The harmonic products at frequencies far removed from f_{Tx} can lead to severe interference for the receivers tuned to those frequencies. The objective here is to model the spurious emission at those frequencies and cancel it on the receiver side, to clean up the received signal. In this way, the transmitter can continue to operate at maximum efficiency, the saw filtering requirements of the system can be substantially relaxed, and the signal to interference plus noise ratio (SINR) of the receiver can be improved.

To accomplish the above tasks we perform analytical derivations for the harmonic emission content, and then suggest non-linear kernels that can model this emission. We derive and generalize these kernels and then set up an ET amplifier test-bench to test the theory on a real RF system. The derivation of kernels is performed in Section II and the results of using these kernels with an experimental setup appear in Section III. We demonstrate through a practical amplifier setup, that cancellation performance of 20–30 dB can be obtained in these scenarios. Some initial experimental investigation has been reported in [14]. Here we derive the

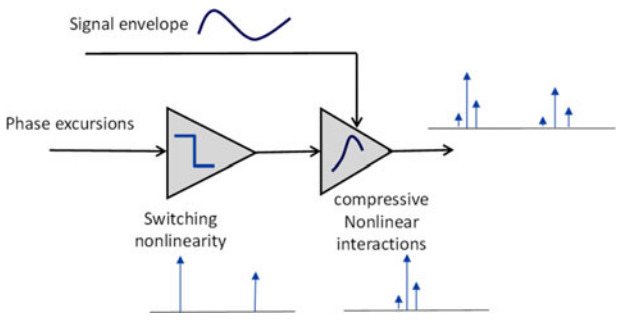

Fig. 2. Physical intuition for non-linear emissions of supply modulation.

https://doi.org/10.1017/S1759078716000933 Published online by Cambridge University Press

mathematical details of kernels, and give details on the possible digital realization of this cancellation scheme, along with the detailed RF measurements on the amplifier test-bench.

II. DIGITAL CANCELLATION SCHEME

The objective of modeling spurious emissions in this work, is to perform receive domain cancellation of these signal components, to enhance operating characteristics of the transceiver. The outline of the proposed digital cancellation setup is shown in Fig. 3. As can be seen from the figure, the dotted line on the spectrum profile refers to the spurious emission derived from Fig. 2, which falls into the receive band. A part of the spurious emission finds its way through finite duplexer attenuation and gets down-converted into the receiver-operating frequencies. This interference is superimposed on the received signal. The blocks and lines in gray (Fig. 2) articulate the proposed cancellation scheme. In this scheme, the signal going into the transmitter is tapped (digitally) and passed through a modeling system, which comes up with an estimate of the non-linear interference falling into the receive-band. The cancellation happens before the receiver's matched filter, and the residual of the cancellation is used to form an adaptive loop to tune the coefficients of the digital modeling system.

Several points are worthy of notice in the proposed cancellation scheme. It can be operated in the calibration or operating mode. In the calibration mode, no receive signal is present on the receive antennae and hence only interference is being used to train the modeling system. However, this is not the only mode of operation, and the adaptation of coefficients can continue even when the received signal is superimposed on top of the interference. This is due to the minimum-mean-square-error criterion (MMSE), which is used in the adaptation loop. MMSE criterion ensures that received signal is treated as a noise for the estimation process. If the adaptation is sufficiently slowed (to increase correlation time and hence signal to noise ratio (SNR)), then this strategy is adequate to recover the interference generating coefficients. The digital modeling system, showed in Fig. 3, is the focus of our work in this paper. This system is required to model the harmonic content at frequencies far removed from the transmission frequency. The paper therefore details the analytical derivation for a kernel required to generate such harmonic content. It then confirms the derivation through a set of system simulations. We give some estimates on the circuit complexity and power consumption required to implement these components by synthesizing them in silicon. The final part shows the RF measurements performed on a real ET amplifier, and applying the modeling equations to predict and cancel the harmonic content captured from the PA test-bench.

III. NON-LINEAR KERNELS FOR HARMONIC EMISSION

We first discuss the derivation of kernels for accurate modeling of third harmonic. In order to do this, we need to first derive the effect of third-order non-linearity on the modulated signal. In order to represent the modulated signal, we use the base-band in-phase and quadrature waveforms, represented by $I(t)$ and $Q(t)$ and modulate them with the carrier signal, which is passed through a non-linearity, after which the base-band representation is again extracted from the signal. We

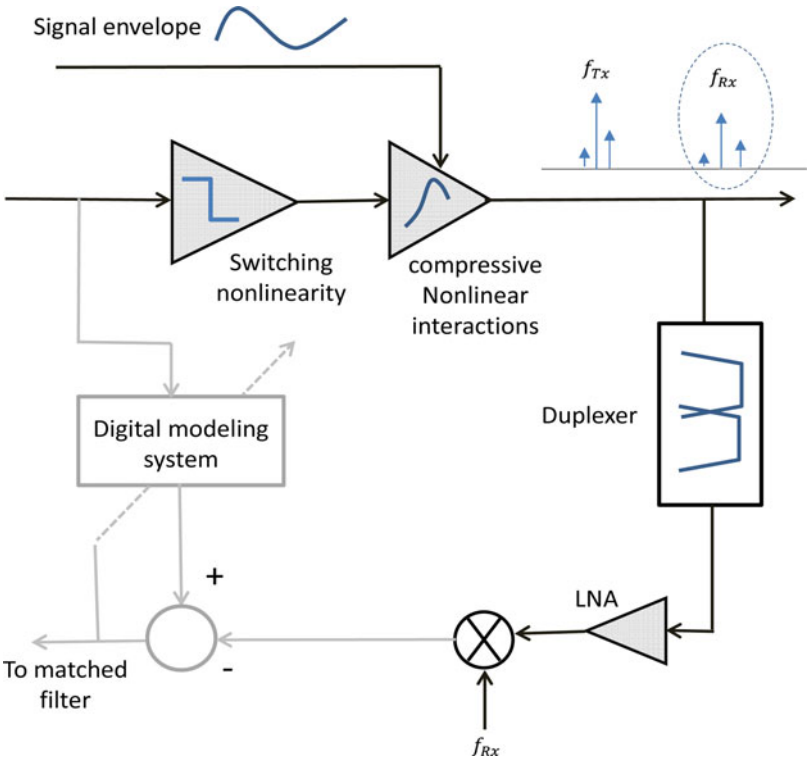

Fig. 3. Proposed digital cancellation system.

https://doi.org/10.1017/S1759078716000933 Published online by Cambridge University Press

then use the extracted representation to create a base-band equivalent model of the third harmonic. Let *Tx*PA input be represented as a function of complex base-band values as follows:

$$TxPAin = I(t)\cos(\omega t) - Q(t)\sin(\omega t). \tag{1}$$

If this signal was to encounter a third-order non-linearity we can write the expansion as follows:

$$\begin{aligned} TxPAin^3 = {} & I(t)^3\cos^3(\omega t) - 3I(t)^2Q(t)\cos^2(\omega t)\sin(\omega t) \\ & + 3I(t)Q(t)^2\cos(\omega t)\sin^2(\omega t) \\ & - Q(t)^3\sin^3(\omega t) \end{aligned} \tag{2}$$

calling the output as Tx^3, the expression can be simplified by using trigonometric identities

$$Tx^3 = \frac{1}{4}\begin{bmatrix} 3\ I(t)^3\cos(\omega t) - 3I(t)Q(t)^2\cos(\omega t) + I(t)^3\cos(3\omega t) \\ +Q(t)^3\sin(3\omega t) + 3I(t)Q(t)^2\cos(3\omega t) - 3Q(t)^3\sin(\omega t) \\ -3I(t)^2Q(t)\sin(3\omega t) \end{bmatrix}. \tag{3}$$

If we apply a filter to collect the third harmonic (centerd at 3ω), (as opposed to collecting the terms for the fundamental as is usually done) we get the terms as shown separately in (4)

$$\begin{aligned} Tx^3_{@3\omega} = H_3 = {} & \frac{1}{4}(I(t)^3 - 3I(t)Q(t)^2)\cos(3\omega t) \\ & - \frac{1}{4}(-3I(t)^2Q(t) + Q(t)^3)\sin(3\omega t). \end{aligned} \tag{4}$$

We observe that coefficients of real and imaginary part no longer relate to the complex base-band model for the fundamental signal component. Assuming a complex base-band representation, we may write the original transmitted signal as

$$x = I(t) - jQ(t). \tag{5}$$

We form a complex number after performing complex multiplications of the number with itself as shown in (6)

$$\hat{H}_{3BB} = (I(t) - jQ(t))^3 = x^3. \tag{6}$$

The power operation shown in (6) is accomplished by performing two complex multiplications. The result is given as a base-band estimate of the non-linear products existing at the third harmonic.

$$\hat{\mathrm{H}}_{3BB} = I(t)(I(t)^2 - 3Q(t)^2) + jQ(t)(-3I(t)^2 - Q(t)^2). \tag{7}$$

The expression in (7) is significant. It tells us that real and imaginary parts of the product exactly correspond to the cosine and sine coefficients in (4). The distortion generated at the third harmonic can be modeled by the complex equivalent base-band model in (7).

It is known from non-linear systems theory that higher-order non-linearities will also create distortion at the location of third harmonic. In order to generalize the modeling of third-order distortion, we need to include higher-order non-linearities. If the receiver is specifically tuned to the frequency of about $3f_{Tx}$, we need to find the order of non-linearity that can generate spectral content at three times the transmit frequency. Raising *Tx* signal to the next available power of 4, and performing trigonometric simplification we obtain

$$Tx^4 = \frac{1}{8}\begin{bmatrix} +3\ I(t)^4 + 6I(t)^2Q(t)^2 + 3Q(t)^4 \\ +(-4I(t)^4 + 4Q(t)^4)\cos(2\omega t) \\ +(8I(t)^3Q(t) + 8I(t)Q(t)^3)\sin(2\omega t) \\ +(I(t)^4 - 6I(t)^2Q(t)^2 + Q(t)^4)\cos(4\omega t) \\ +(-4I(t)^3Q(t) + 4I(t)Q(t)^3)\sin(4\omega t) \end{bmatrix}. \tag{8}$$

We observe that this leads to distortion products at the DC as well as at two times and four times the transmit frequency. These distortion products are not relevant for the receiver tuned about $3f_{Tx}$. When we raise the *Tx* signal to the next odd power of 5, we obtain distortion products at the third harmonic. This is shown in (9).

$$Tx^5 = \frac{1}{16}\begin{bmatrix} (10I(t)^5 + 20I(t)^3Q(t)^2 + 10I(t)Q(t)^4)\cos(\omega t) \\ +(-10I(t)^4Q(t) - 10I(t)^2Q(t)^3 + 5Q(t)^5)\sin(\omega t) \\ +(5I(t)^5 - 10I(t)^3Q(t)^2 - 15I(t)Q(t)^4)\cos(3\omega t) \\ +(-15I(t)^4Q(t) - 10I(t)^2Q(t)^3 + 5Q(t)^5)\sin(3\omega t) \\ +\text{Higher Harmonic Terms} \end{bmatrix}. \tag{9}$$

Paying careful attention to the third-harmonic terms, we try to reconstruct it using the base-band signal of (5). A first guess would yield a base-band estimator of the form.

$$\hat{\mathrm{H}}_{3BB}(5^{th}) = (I(t) - jQ(t))^5. \tag{10}$$

Interestingly, the estimator of (10) does not yield the correct coefficients. Expanding (10) yields,

$$\begin{aligned} \hat{\mathrm{H}}_{3BB}(5^{th}) = {} & (I(t)^5 - 10I(t)^3Q(t)^2 + 5I(t)\mathrm{Q}(t)^4) \\ & + j(5I(t)^4Q(t) - 10I(t)^2Q(t)^3 + Q(t)^5). \end{aligned} \tag{11}$$

Comparing the cosine and sine coefficients of third harmonic in (9) with the real and imaginary parts of (11) respectively will tell us that (10) is not the correct non-linear model for estimating the third-order coefficients. The correct base-band model turns out to be

$$\hat{\mathrm{H}}_{3BB}(5^{th}) = (I(t) - jQ(t))^3\ |I(t) - jQ(t)|^2, \tag{12}$$

which when expanded leads to the real and imaginary parts as shown in (12)

$$\begin{aligned} \hat{\mathrm{H}}_{3BB}(5^{th}) = {} & (I(t)^5 - 2\mathrm{I}(t)^3Q(t)^2 - 3I(t)Q(t)^4) \\ & + j(-3I(t)^4Q(t) - 2I(t)^2Q(t)^3 + Q(t)^5), \end{aligned} \tag{13}$$

which exactly match the cosine and sine terms of the third harmonic in (9) (within a scale factor). Similarly we calculated the contribution to third harmonic by the impact of seventh-order non-linearity and found that the coefficients

https://doi.org/10.1017/S1759078716000933 Published online by Cambridge University Press

can be given by

$$\hat{H}_{3BB}(7^{th}) = (I(t) - jQ(t))^3\ |I(t) - jQ(t)|^4. \quad (14)$$

This leads us to postulate for the first time in the non-linear literature, that the third harmonic located at $3f_{Tx}$ can be modeled using non-linear kernels of the form

$$\hat{H}_{3BB}(n) = (I(t) - jQ(t))^3\ |I(t) - jQ(t)|^{(n-3)},\ n = 3, 5, 7, \ldots. \quad (15)$$

We can further postulate that any odd-order harmonic can be modeled using non-linear kernels of the form

$$\hat{H}_{kBB}(n) = (I(t) - jQ(t))^k\ |I(t) - jQ(t)|^{(n-k)},\quad n = k + 3, k + 5, k + 7, \ldots. \quad (16)$$

In order to learn how the spectral emission behaves in terms of its bandwidth, we can use two tones to excite the non-linearity and observe the impact on the resulting harmonics [15]. Let ω_1 and ω_2 constitute the two input frequencies to the non-linearity. Our input signal is therefore given by

$$TxPAin = \cos(\omega_1 t) + \sin(\omega_1 t) + \cos(\omega_2 t) + \sin(\omega_2 t). \quad (17)$$

After passing the above signal through a third-order non-linearity exactly similar to (2) we can write the resulting components of the output as follows:

$$\begin{aligned} Tx^3 = {} & \frac{1}{2}(9\cos(\omega_1 t) - \cos(3\omega_1 t) + 9\cos(\omega_2 t) - \cos(3\omega_2 t)) \\ & + \frac{1}{2}(3\cos(\omega_1 t - 2\omega_2 t) - 3\cos(2\omega_1 t - \omega_2 t) \\ & - 3\cos(\omega_1 t + 2\omega_2 t) - 3\cos(2\omega_1 t + \omega_2 t)) \\ & + \text{Similar } \sin(\omega t) \text{ terms}. \end{aligned} \quad (18)$$

From the above expression, we collect the terms close to the third-harmonic frequency and write the expression as

$$\begin{aligned} Tx^3_{@3\omega} = {} & \frac{1}{2}(-\cos(3\omega_1 t) - \cos(3\omega_2 t)) + \frac{1}{2}(3\cos(\omega_1 t + 2\omega_2 t) \\ & - 3\cos(2\omega_1 t + \omega_2 t)) + \text{Similar } \sin(\omega t) \text{ terms}. \end{aligned} \quad (19)$$

We observe from (19) that frequency components located close to the third harmonic, start from $3\omega_1$, span over $2\omega_1 + \omega_2$ and $2\omega_2 + \omega_1$, and finish off at the maximum value of $3\omega_2$. Therefore the bandwidth of the frequency content located at this harmonic is $3\omega_2 - 3\omega_1$. We conclude that the bandwidth is three times the fundamental bandwidth (given by tone spacing of $\omega_1 - \omega_2$).

We can do steps similar to the third-harmonic modeling to do model the second harmonic. The next section performs these steps and concludes the general expression for modeling the signal content at the second-harmonic frequency.

IV. KERNEL DERIVATION FOR MODELING EVEN HARMONICS

For the modeling of second harmonic we consider a *Tx* signal similar to (1). After passing the signal through a second-order non-linearity we incur a harmonic expansion given as follows:

$$\begin{aligned} (TxPAin)^2 = {} & \frac{1}{2}\ (I(t)^2 + Q(t)^2 + [Q(t)^2 - I(t)^2]\cos(2\omega t) \\ & - 2I(t)Q(t)\sin(2\omega t)). \end{aligned} \quad (20)$$

After extracting the second harmonic we can write the signal appearing at the harmonic frequency as,

$$\begin{aligned} Tx^2_{@2\omega} = {} & \frac{1}{2}(Q(t)^2 - I(t)^2)\ \cos(2\omega t) \\ & - I(t)Q(t)\sin(2\omega t). \end{aligned} \quad (21)$$

We can now test the kernel formulation by forming a kernel using a complex base-band equivalent signal of the form shown in (5). Forming a squared distortion from original signal we can write

$$\hat{H}_{2BB} = x^2 = (I(t)^2 - Q(t)^2) - jQ(t)I(t). \quad (22)$$

Neglecting scalar gains, we observe that (22) has the real and imaginary parts, which exactly correspond to the cos and sin coefficients in (20), respectively. Similar reasoning also goes for writing the impact of higher-order non-linearities on the second harmonic; so that we can take the intuition developed through 20–22 and write the expression for harmonic emission due to a fourth-order non-linearity as,

$$\begin{aligned} \hat{H}_{2BB}(4^{th}) = {} & x^2|x|^2 \\ = {} & (I(t)^4 - Q(t)^4) - j2(I(t)^3Q(t) + Q(t)^3I(t)). \end{aligned} \quad (23)$$

The real and imaginary components in the above equation check out with the fourth-order expansion in (8) when looking at the second-order terms. We can therefore write an expression for the generalized formulation for the second-order harmonic emission using non-linear kernels as follows:

$$\hat{H}_{2BB}(n) = (I(t) - jQ(t))^2\ |I(t) - jQ(t)|^{(n-2)},\ n = 2, 4, 6, \ldots. \quad (24)$$

We can use (24) to create interference estimate for harmonic content located at the far off second-harmonic frequency. Different orders of non-linearity can be accommodated by changing values of n in the expression.

V. ESTIMATION SYSTEM FOR HARMONIC EMISSION

The third- and second-harmonic modeling have been detailed out in the earlier sections. We can now use equations (15) and (22) to model the signal content at harmonic frequencies. The

https://doi.org/10.1017/S1759078716000933 Published online by Cambridge University Press

signal content at the second harmonic can be written as

$$y = \sum_{k=2}^{K} a_k \hat{\mathrm{H}}_{2BB}(k), \quad k = 2, 4, 6, \tag{25}$$

where a_k are the coefficients of different kernel orders.

Our objective is to determine the emission coefficients a_k's such that we are able to reproduce the emission content y precisely. We can take our clue from the kernel estimation theory. We know that harmonic emission is a result of a non-linear transformation on the input signal x. If we consider our input signal to be $x(t)$, than the second-harmonic component can be generated through any number of non-linear kernels represented by ϕ_k as shown below:

$$H_{2BB}(k) = x^2(n)|x(n)|^{k-2}, \quad k = 2, 4, 6, \ldots, \mathbf{K}. \tag{26}$$

We note that the kernel above is only a memoryless non-linearity. Although including memory would enhance the modeling accuracy of these kernels, we limit our discussion in this paper to memoryless kernels, and also show that remarkably good performance can be achieved by just using memoryless non-linearity. Let

$$\phi_k(n) = x^2(n)|x(n)|^{k-2}. \tag{27}$$

The kernel is now represented through a non-linear operator ϕ_k, where k represents the order of the operator. The operator acts on the input signal $x(n)$ to transform it non-linearly. We can setup an optimization criterion to select a_k's according to the least-squares error minimization.

Representing the received signal $y(n)$ as a time series vector, and breaking that vector into a result of matrix–vector multiplication of kernels and coefficients we can write it as a vector matrix equation. In the matrix equations below (28), the argument of ϕ_k has been shown as just a number, n, ranging from 1 to N. However, that is only shown here for simplicity. The number inside the argument of ϕ_k actually represents the time sample $x(n)$ at the instant n. This is also clear from (27) which shows the argument of ϕ_k as n only, but the signal is actually composed of samples $x(n)$.

The vector matrix equation can be formulation as a set of vectors and matrices shown as Y, $\mathbf{\Phi}$, and A. The set of equations can then be solved for the vector A using least squares formulation, as shown below.

$$\underbrace{\begin{bmatrix} y(1) \\ y(2) \\ . \\ . \\ . \\ y(N) \end{bmatrix}}_{Y} = \underbrace{\begin{bmatrix} \phi_k(1) & \phi_{k+2}(1) & . & . & . \\ \phi_k(2) & \phi_{k+2}(2) & & & \\ . & & . & & \\ . & & & . & \\ . & & & & \\ \phi_k(N) & . & . & . & \phi_K(N) \end{bmatrix}}_{\Phi} \underbrace{\begin{bmatrix} a_1 \\ a_2 \\ . \\ . \\ . \\ a_3 \end{bmatrix}}_{A}. \tag{28}$$

Then

$$A = [\boldsymbol{\Phi}^H \boldsymbol{\Phi}]^{-1} \boldsymbol{\Phi}^H Y. \tag{29}$$

We observe that a_k's are selected to minimize the difference between the weighted non-linearly transformed version of the input and the actual emission seen at the receiver. The use of above technique would be called batch least squares.

However, using the same optimization criterion we can also use stochastic gradient methods to operate on the streaming data samples. In this mode, we can transform the immediate value of $x(n)$ through a non-linear kernel to form a vector $X_{\phi_k}(n)$ where k in ϕ_k varies from $1-\mathbf{K}$ in increments of 2

$$x(n) \rightarrow \phi_{\mathrm{k}}(n) \rightarrow \left[X_{\phi_k}\right], \quad k = 1, \ldots., \mathbf{K}, \tag{30}$$

where X_{ϕ_k} is a vector. The update for coefficients a_k's can be written as a Newton-type update using the gradient of the optimization function

$$\arg \min_{\hat{a}_n} \left[y(n) - X_{\Phi_k}(n)\, \hat{a}_k(n)\right]. \tag{31}$$

The above optimization function shows to select a_k's which minimize the instantaneous value of the objective function. A Newton-type update would be given as

$$a_k(n+1) = a_k(n) + \nabla_{\text{objective function}}, \tag{32}$$

which can be converted using a first-order approximation model to

$$a_k(n+1) = a_k(n) + \mu e X_{\phi_k}, \tag{33}$$

where μ is the adaptation factor and e is the error between estimated and observed interference, that is $e = y - X_{\Phi_k}(n)a_k(n)$. A lower value of μ will lead to slow convergence but lower steady-state error. A higher value of μ would lead to faster convergence and more variation in the value of estimated coefficients.

We observe that all the non-linear kernels derived so far are memoryless. They do not use any variation of the time delayed version of the input. A non-linear kernel using memory effect would be of the form $\phi_k(n) = x^2(t)x(t-\tau)$. Such kernels are indeed possible, and highly likely in large (device size) PAs with complex non-linear switching mechanisms. The principal problem with expansions involving memory is the curse of dimensionality. The coefficients needed to tune this kind of model grow exponentially with the order of the polynomial used. Hence the adaptation becomes computationally very intensive. Although better residual error performance will be obtained using these models, we have chosen to use memoryless models for this paper so that tuning complexity remains manageable.

A simulation setup to test the derivation of kernels and modeling with them is shown in Fig. 4. The upper signal chain of the figure is used to model actual harmonic generation, whereas lower signal chain is used to form the estimation of harmonic interference. In the upper signal chain, a transmit signal is passed through a tangent hyperbolic function to excite non-linearities of different odd orders. The signal is up-converted using $e^{+j\omega t}$ and then passed through a second-order non-linearity, which is followed by a down-conversion with $e^{-j2\omega t}$ and filtered to capture the second harmonic of transmission.

https://doi.org/10.1017/S1759078716000933 Published online by Cambridge University Press

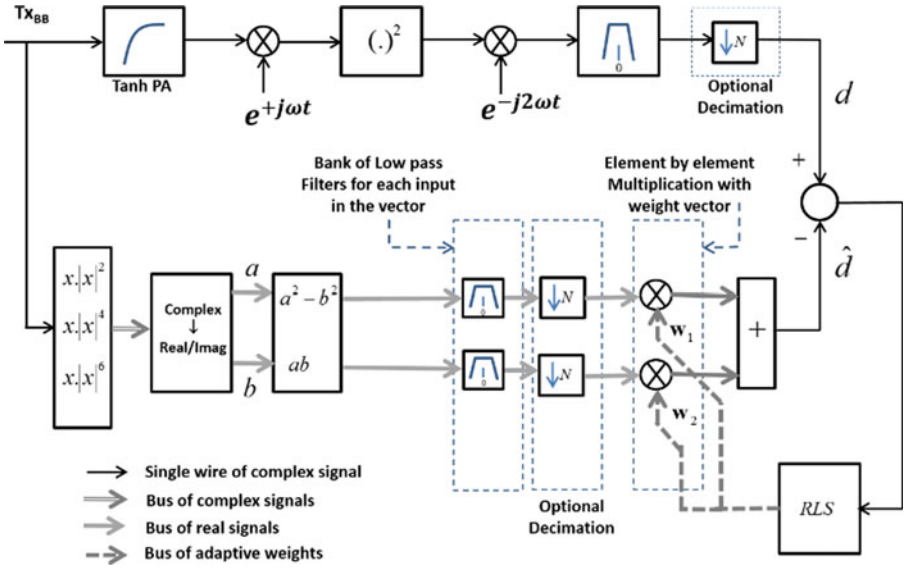

Fig. 4. System used to model the second-harmonic cancellation.

The non-linearly distorted transmit signal and the signal after second-order non-linearity are shown in Fig. 5. The signal is up-converted to the frequency of 80 MHz and the second-order non-linearity results in distortion present at the base-band and second harmonics. One of these harmonics is down-converted to the base-band and used as the second-harmonic emission sampled by the receiver.

In the bottom branch of Fig. 4, we first use the *Tx* signal to form a volterra series for odd-order non-linearities that create adjacent channel spectral expansion. The resulting complex vector is then processed to create a second-order effect as given in (23). The vector of second-order estimators is multiplied with a set of weights called w_1 for real signals and w_2 for imaginary signals in the figure. The original transmit signal used in the simulation is an LTE waveform having a bandwidth of 5 MHz. The results of passing this waveform through a non-linear function and a second-order distorter along with subsequent cancellation are shown in Fig. 6.

Figure 6 shows the results of cancellation of second harmonic using second and third-order volterra filters. Second-order filter signifies having a linear and a third-order kernel, along with $(.)^2$ order estimator to estimate the second-harmonic emission. Similarly, third-order filter uses linear, third and fifth-order kernels along with $(.)^2$ order estimator to estimate emission. We see that main lobe of the second-harmonic emission spans 10 MHz (two times the original bandwidth of 5 MHz) and the second-order filter is able to cancel the entire main lobe of harmonic content. The residual of cancellation is 30 dB down in this case. Increasing the order of the volterra kernel by 1, leads to a residual emission, which is 45 dB down. The simulation results show that the technique can indeed be used to cancel the harmonic emission content. Section VI will discuss the implementation complexity of the approach and Section VII will show the validation of the scheme using measurements on actual RF amplifier test-bench.

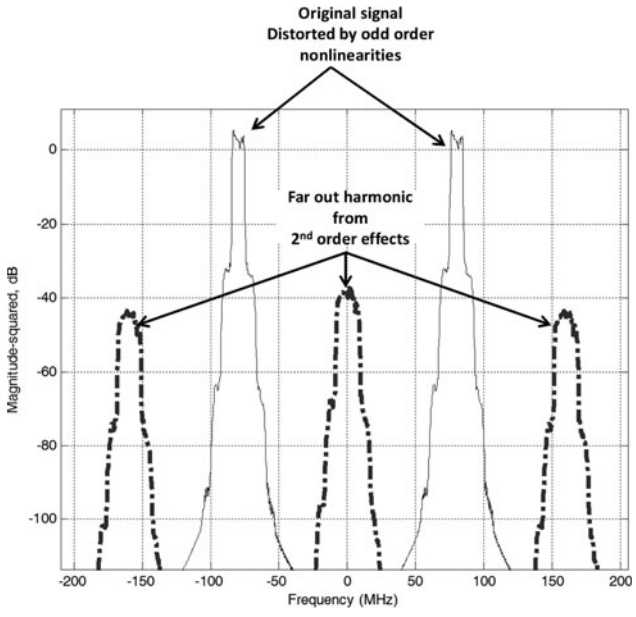

Fig. 5. Odd-order non-linear distortion and second harmonics.

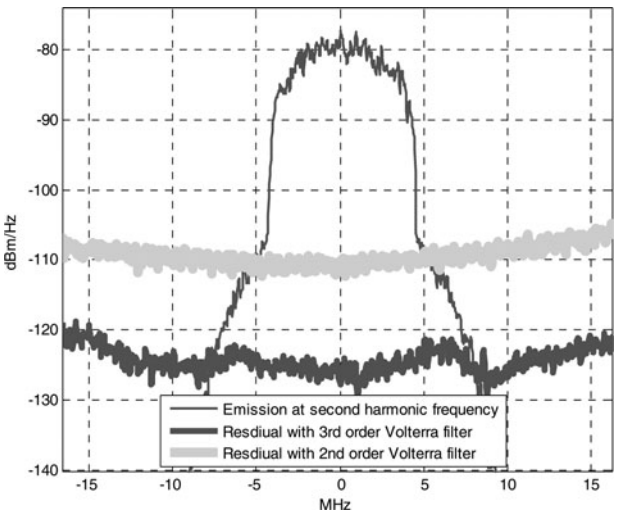

Fig. 6. Simulation results for second-harmonic cancellation.

https://doi.org/10.1017/S1759078716000933 Published online by Cambridge University Press

VI. POWER AND COMPUTATIONAL REQUIREMENTS

This section will address the computational requirements of the proposed cancellation methodology. The circuit level power consumption will be derived, and some analysis on the chip-scale behavior of the system will be conducted. This analysis is however geared toward providing the practical bounds on performance of the system, rather than absolutely certain numbers. The actual area and power consumption of the chip will vary. We will discuss the behavior exhibited by our VLSI and custom processor implementation, and will provide guidelines on the implementation. The measurement section will however evaluate the system with actual RF hardware, but without the customized digital implementation. Digital processing on the bench will be carried out off-line with a normal computing platform.

The digital VLSI hardware consists of polynomial generators and complex multipliers multiplying each polynomial term. A polynomial of maximum degree N can be synthesized by taking a magnitude, and raising magnitude to even powers and finally multiplying with the complex input. It can be implemented using a CORDIC block which takes the magnitude, and subsequently squares or cubes the magnitude and finally multiples the result with the actual complex number to generate polynomials of various orders. These polynomial terms are then multiplied with the coefficients computed for each term (using the adaptation algorithms described earlier). The circuit therefore consists of three main digital blocks of CORDIC, Polynomial Generator, and multiplier array to comprise the interference estimation module. The complete circuit was designed in Simulink and converted to HDL using the HDL coder. The synthesized circuit was then run in a realistic cancellation simulation, and activity of different gates was recorded. The activity level was given to the synopsis power estimation tools to determine the dynamic and static power consumption. The results are shown in Table 1.

As we can see, the entire circuit ends up consuming nearly 2 mW of power. This is very little penalty to pay for extra power consumed by the PA due to duplexer losses. We can end up saving nearly 50 mW of power by resorting to the non-linear cancellation. For the above digital implementation, the design used 773 flip flops and occupied an area of 0.04 sqmm in a CMOS 40 nm process node.

VII. MEASUREMENTS AND EXPERIMENTAL VALIDATION

In order to validate the derivation of the kernel for second and third-harmonic emission, we setup an experimental test-bench with the ET PAs. The test-bench consists of an ET PA optimized for efficiency, and a harmonic capture and digitizing board. A base-band transmit signal is split into a main signal component which is up-converted to the RF frequency, and a low-frequency envelope modulation component. These two are individually fed to an ET amplifier and care is taken to maintain precise synchronization between the two signals. This is maintained by fractional rate interpolation inside the signal processing chain. A farrow interpolator is used to provide fine synchronization on a five times oversampled waveform. The oversampling ratio of five is selected to make the task of precise synchronization easier to accomplish. Additional calibrations include I/Q imbalance cancellation, and frequency offset cancellation for the transceiver. I/Q imbalance is calibrated using adaptive equalizer for side-band suppression, whereas frequency offset is removed through a modified costas loop. The harmonics generated from ET amplifier remain unattenuated due to lack of any filtering in the system. The output signal carrying the harmonic content is taken to the 'Harmonic Capture and Digitizing Board' where is it mixed with an LO signal of the harmonic frequency, down-converted to base-band and sampled by the ADCs. The setup is shown in Fig. 7.

Typical bandwidths of the signal used range from 5 to 10 MHz of LTE signal, whereas the sampling of the harmonics is performed at 127 MSa/s. This allows all the harmonic content along with its non-linear spectral expansion to be captured conveniently. The captured bandwidth is resampled digitally inside our digital signal processing (DSP) system. Our DSP system consists of a PC running accelerated Matlab on GPU processing units. The version of the algorithm used for tuning final coefficients is recursive least squares (RLS) with a forgetting factor of 0.99. Figure 7 shows the cancellation and signal processing portion of the system on the top of the figure. We observe that the original Tx base-band signal is passed through the kernel generation process to generate non-linear kernels of different orders. These kernels are then multiplied by adaptive weights and subsequently linearly combined to generate an estimate of the harmonic interference captured through the system. The estimate of the third harmonic is referred to as $\hat{h}_3$ in the figure. The estimate is subtracted from the actual signal h_3 to form the residual which is used to adjust the adaptive weights before the linear combiner.

The original LTE signal versus the captured second and third harmonic are shown in Fig. 8. Each periodogram has been normalized to the same power level in order to provide a comparison between different bandwidths. We observe that the second harmonic has two times the original signal bandwidth of 5 MHz and third harmonic has three times the original bandwidth. Now we can use the modeling of harmonics to cancel them and look at the residual of cancellation. The experiment is performed using only three kernel coefficients. The results of the experiment performed with second harmonic are shown in Fig. 9.

From Fig. 9 we can observe that only with three coefficients we can achieve approximately 20 dB of cancellation performance. The integrated performance over the entire bandwidth can be defined using a Tx_MSE metric which can be written as follows:

$$Tx\_MSE_{dB} = -1 * 10 \log_{10} \frac{E[(h_2 - \hat{h}_2)^2]}{E[(h_2)^2]} . \quad (34)$$

Table 1. Current consumption summary of interference estimation block.

Block	Switching power (mW)	Internal power (mW)	% of total
CORDIC block	0.417	0.309	36.3
Polynomial generator	0.244	0.430	33.7
Multiplier block	0.212	0.385	29.8
Total	0.873	1.124	100.0

https://doi.org/10.1017/S1759078716000933 Published online by Cambridge University Press

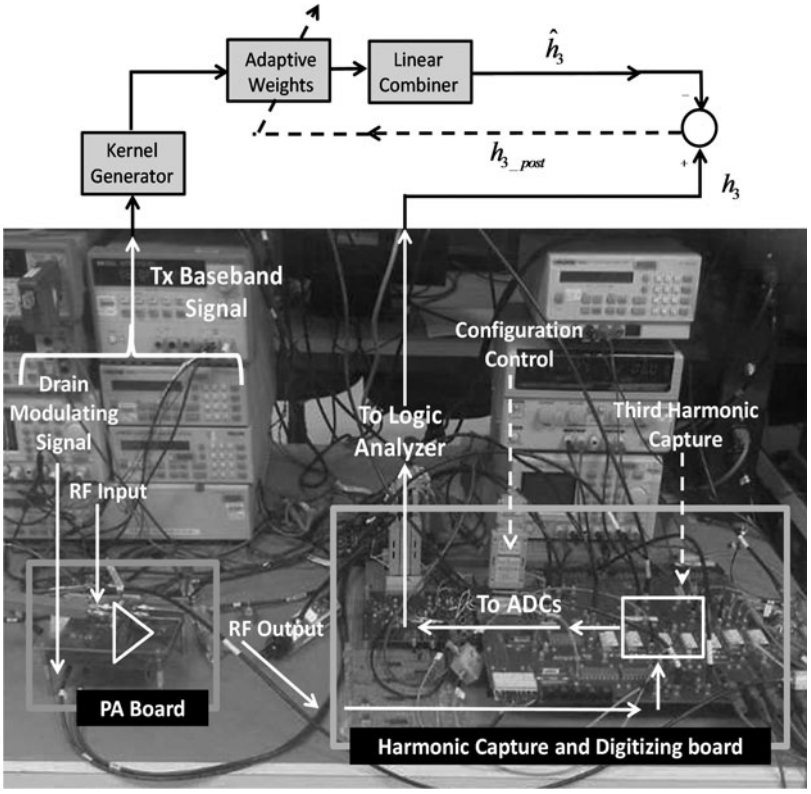

Fig. 7. Test setup for validating cancellation performance.

The results of Fig. 9, when mapped to the criterion of (34), the system shows nearly 17 dB of *Tx_MSE* performance. The board was then configured to capture the third harmonic, and the adaptive system shown in Fig. 7 was used to estimate and cancel the third harmonic of the LTE waveform. The results of the exercise are shown in Fig. 10, which shows that the main lobe of third harmonic does indeed occupy three times the bandwidth of the original signal.

The cancellation obtained in Fig. 10 is achieved using three adaptive kernel terms. The recorded MSE of the system is 3.72 dB, which signifies that the power of the residual terms is 5 dB lower than the original harmonic. Although the integrated power (over the entire bandwidth) is only ∼4 dB lower, we have obtained better cancellation for the signal content close to DC and lower frequencies. The cancellation performance can be vastly improved using more kernels terms. Three set of experiments were conducted using different kernel terms and the results are summarized in Fig. 11.

We observe from Fig. 11 that more than 10 dB of cancellation has been achieved with eight kernel terms. The actual

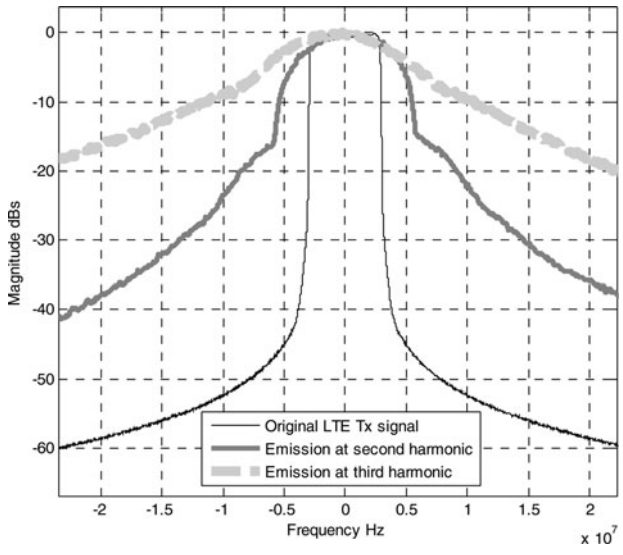

Fig. 8. Original signal versus second and third harmonics.

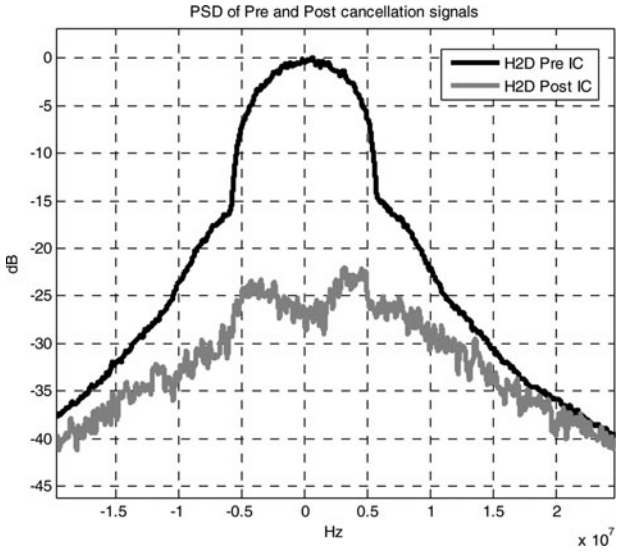

Fig. 9. Cancellation performance with second harmonic.

https://doi.org/10.1017/S1759078716000933 Published online by Cambridge University Press

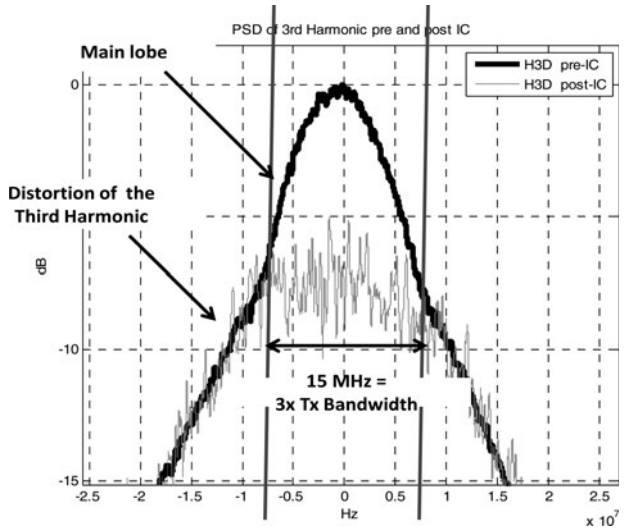

Fig. 10. Cancellation performance with third harmonic.

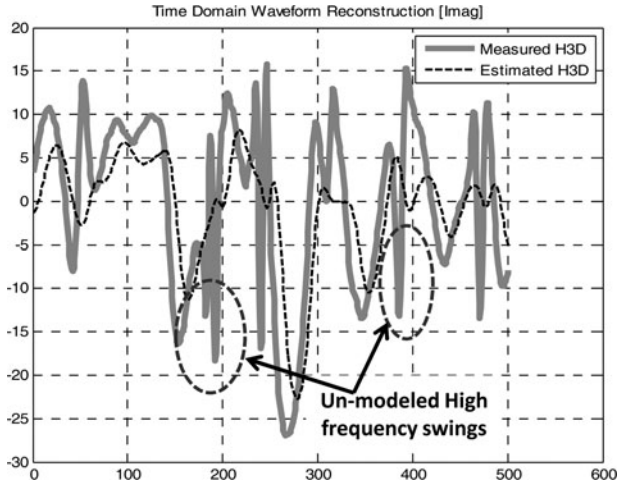

Fig. 12. Time-domain reconstruction with three kernels.

value of means-square error (MSE) from eight terms is 9.75 dB. The difference in modeling can also be observed in time domain, and can also be helpful in recognizing when the order of the estimation system needs to be increased. In order to illustrate this difference, the time waveform of laboratory captured and estimated harmonic are superimposed on each other for the systems with three and eight kernels. The results are shown in Figs 12 and 13.

From the reconstruction in Fig. 12, one maybe be led to believe that there is some alignment or synchronization error between the captures and modeled harmonic. The high-frequency swings are not well-modeled and low-frequency swings seem out of phase.

But in Fig. 13, the exact same synchronization scheme is used, while the order of estimation has been increased to eight terms. We observe now that the system begins to catch and model the high-frequency swings, whereas the low-frequency content also seems to be in perfect alignment

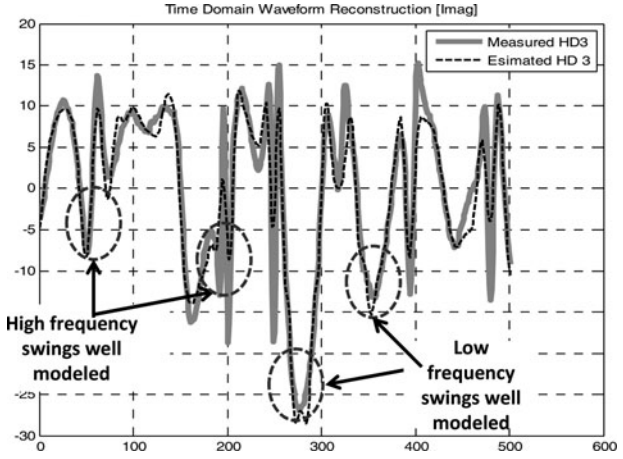

Fig. 13. Time-domain reconstruction with eight kernels.

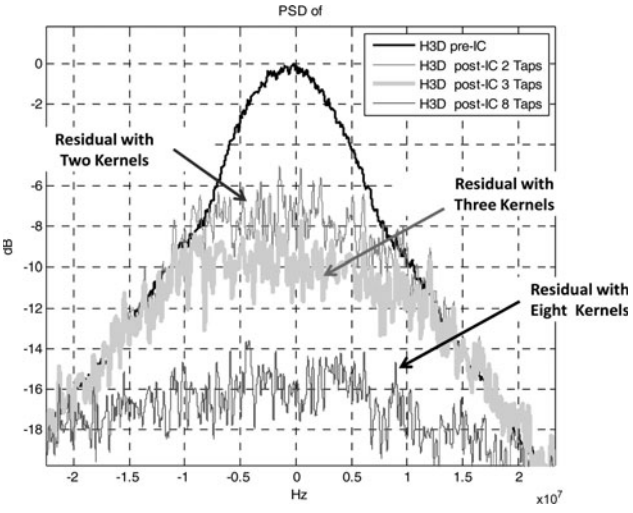

Fig. 11. Third-harmonic cancellation with different kernels.

Table 2. Cancellation performance.

Harmonic frequency	Kernel terms	Cancellation achieved (dB)
$2f_{Tx}$	3	20
$2f_{Tx}$	5	25
$3f_{Tx}$	3	4
$3f_{Tx}$	8	10

between the captured and estimated waveform. We can conclude that the intermodulation terms of the first harmonic also appear as intermodulation at higher harmonics which significantly expand their bandwidth. The additional frequency content can be modeled by non-linear terms as derived in this paper. The addition of such non-linear kernels leads to accurate reconstruction of the original harmonic waveform and can result in significant cancellation of the harmonic.

The harmonic cancellation achieved using different kernel orders for different harmonic content location is summarized in Table 2.

https://doi.org/10.1017/S1759078716000933 Published online by Cambridge University Press

VIII. CONCLUSION

In this paper, we look at the problem of spurious transmitter emission at higher-harmonic frequencies. The non-linear models for predicting this kind of interference are non-existent in the literature. We provide a derivation of the kernel for such an emission, and then use the derived kernels to predict actual interference coming from a laboratory setup. We derived the kernels for emission at the second- and third-harmonic frequency and generalized the kernels to include the effect of higher-order non-linearities. The theoretical model is well able to predict actual interference and provide a very good cancellation performance to validate the theory with laboratory measurements. This allows this estimation scheme to be used in conjunction with very high-efficiency ET transmitters, which generate significant second and third harmonics.

ACKNOWLEDGEMENTS

The authors would like to thank SSE LUMS, and radio technology laboratories at Qualcomm where parts of this work have been carried out.

REFERENCES

[1] Kim, J.; Son, J.; Jee, S.; Kim, S.; Kim, B.: Optimization of envelope tracking power amplifier for base-station applications. IEEE Trans. Microw. Theory Tech., **61** (4) (2013), 1620–1627.

[2] Zhou, G.T.: Analysis of spectral regrowth of weakly nonlinear power amplifiers, in IEEE Int.l Conf. on Acoustics, Speech, and Signal Processing, Proceedings, vol. **5,** 2000, 2737–2740.

[3] Ku, H.; Kenney, J.S.: Behavioral modeling of RF power amplifiers considering IMD and spectral regrowth asymmetries, in IEEE MTT-S Int. Microwave Symp. Digest, vol. **2,** 2003, 799–802.

[4] Gard, K.G.; Gutierrez, H.M.; Steer, M.B.: Characterization of spectral regrowth in microwave amplifiers based on the nonlinear transformation of a complex Gaussian process. IEEE Trans. Microw. Theory Tech., **47** (7) (1999), 1059–1069.

[5] Omer, M.; Rimini, R.; Heidmann, P.; Kenney, J.S.: A compensation scheme to allow full duplex operation in the presence of highly nonlinear microwave components for 4 G systems, in IEEE MTT-S Int. Microwave Symp. Digest (MTT), 2011, 1–4.

[6] Omer, M.; Rimini, R.; Heidmann, P.; Kenney, J.S.: A PA-noise cancellation technique for next generation highly integrated RF front-ends, in IEEE Radio Frequency Integrated Circuits Symp. (RFIC), Montreal, QC, 2012, 471–474.

[7] Zhou, J.; Chakrabarti, A.; Kinget, P.R.; Krishnaswamy, H.: Low-noise active cancellation of transmitter leakage and transmitter noise in broadband wireless receivers for FDD/co-existence. IEEE J. Solid-State Circuits, **49** (12) (2014), 3046–3062.

[8] Razavi, B.: The future of radios, in IEEE Int. Symp. on Circuits and Systems (ISCAS), 2015, 1–8.

[9] Fabiano, I.; Sosio, M.; Liscidini, A.; Castello, R.: SAW-less analog front-end receivers for TDD and FDD. IEEE J. Solid-State Circuits, **48** (12) (2013), 3067–3079.

[10] Goel, A.; Analui, B.; Hashemi, H.: Tunable duplexer with passive feed-forward cancellation to improve the RX-TX isolation. IEEE Trans. Circuits Syst. I: Regul. Pap., **62** (2) (2015), 536–544.

[11] Schafer, S.; Popovic, Z.: Multi-frequency measurements for supply modulated transmitters. IEEE Trans. Microw. Theory Tech., **63** (9) (2015), 2931–2941.

[12] Raffo, A.; Bosi, G.; Vadala, V.; Vannini, G.: Behavioral modeling of GaN FETs: a load-line approach. IEEE Trans. Microw. Theory Tech., **62** (1) (2014), 73–82.

[13] Santarelli, A.; Di Giacomo, V.; Raffo, A.; Traverso, P.A.; Vannini, G.; Filicori, F.: A nonquasi-static empirical model of electron devices. IEEE Trans. Microw. Theory Tech., **54** (12) (2006), 4021–4031.

[14] Omer, M.; Rimini, R.; Draxler, P.J.; Kenney, J.S.: Interference cancellation for odd harmonics of envelope tracking RF power amplifier systems, in IEEE MTT-S Int. Microwave Symp. Digest (IMS), 2013, 1–3.

[15] Ku, H.; Mckinley, M.D.; Kenney, J.S.: Extraction of accurate behavioral models for power amplifiers with memory effects using two-tone measurements, in IEEE MTT-S Int. Microwave Symp. Digest, vol. **1,** 2002, 139–142.

Mohammad Omer recieved his Masters and Ph.D. degrees in engineering from Georgia Institute of Technology. He has worked with the research divisions of Intel, Qualcomm, and Blackberry developing and contributing to a range of RFIC and signal processing products. Currently he works as a research scientist with Cognitive Systems trying to develop smart radio sensing technology for a wide array of potential applications.

Farasat Munir received his B.S. degree in Electrical Engineering from the University of Engineering and Technology, Lahore, Pakistan. He later received Fulbright scholarship and went to Georgia Institute of Technology, Atlanta, USA, where he earned his Ph.D. in Electrical Engineering in 2012. He is currently working as an Assistant Professor in the Department of Electrical Engineering at SBA School of Science and Engineering LUMS, Pakistan. His research interests include biosensors, biomedical instrumentation, RF, and Microwave circuits.

https://doi.org/10.1017/S1759078716000933 Published online by Cambridge University Press